Available online at www.sciencedirect.com

ScienceDirect

www.elsevier.com/locate/jes

JES JOURNAL OF ENVIRONMENTAL SCIENCES

www.jesc.ac.cn

Measurement of HONO flux using the aerodynamic gradient method over an agricultural field in the Huaihe River Basin, China☆

Fanhao Meng[1,2], *Min Qin*[1,*], *Wu Fang*[1], *Jun Duan*[1], *Ke Tang*[1,2], *Helu Zhang*[1,2], *Dou Shao*[1,2], *Zhitang Liao*[1,2], *Yan Feng*[4,5], *Yong Huang*[4,5], *Ting Ni*[4,5], *Pinhua Xie*[1,2,3], *Jianguo Liu*[1,2,3], *Wenqing Liu*[1,2,3]

[1] *Key Laboratory of Environmental Optics and Technology, Anhui Institute of Optics and Fine Mechanics, Hefei Institutes of Physical Science, Chinese Academy of Sciences, Hefei 230031, China*
[2] *University of Science and Technology of China, Hefei 230026, China*
[3] *Center for Excellence in Regional Atmospheric Environment, Institute of Urban Environment, Chinese Academy of Sciences, Xiamen 361021, China*
[4] *Anhui Institute of Meteorological Sciences, Anhui Province Key Laboratory of Atmospheric Science and Satellite Remote Sensing, Hefei 230031, China*
[5] *Shouxian National Climatology Observatory, Huaihe River Basin Typical Farm Eco-meteorological Experiment Field of China Meteorological Administration, Shouxian 232200, China*

ARTICLE INFO

Article history:
Received 10 May 2021
Revised 29 August 2021
Accepted 6 September 2021
Available online 21 February 2022

Keywords:
Aerodynamic gradient method
HONO flux
Huaihe River Basin
Agricultural field

ABSTRACT

To investigate nitrous acid (HONO) levels and potential HONO sources above crop rotation fields. The HONO fluxes were measured by the aerodynamic gradient (AG) method from 14 December 2019 to 2 January 2020 over an agricultural field in the Huaihe River Basin. The ambient HONO levels were measured at two different heights (0.15 and 1.5 m), showing a typical diurnal cycle with low daytime levels and high nighttime levels. The upward HONO fluxes were mostly observed during the day, whereas deposition dominated at night. The diurnal variation of HONO flux followed solar radiation, with a noontime maximum of 0.2 nmol/(m^2•sec). The average upward HONO flux of 0.06 ± 0.17 nmol/(m^2•sec) indicated that the agricultural field was a net source for atmospheric HONO. The higher HONO/NO_2 ratio and NO_2–to–HONO conversion rate close to the surface suggested that nocturnal HONO was formed and released near the ground. The unknown HONO source was derived from the daytime HONO budget analysis, with an average strength of 0.31 ppbV/hr at noontime. The surface HONO flux, which was highly correlated with the photolysis frequency $J(NO_2)$ (R^2 = 0.925) and the product of $J(NO_2)$ × NO_2 (R^2 = 0.840), accounted for ~23% of unknown daytime HONO source. The significant correlation between HONO fluxes and $J(NO_2)$ suggests a light-driven HONO formation mechanism responsible for the surface HONO flux during daytime.

☆ This article is dedicated to Professor Dianxun Wang.

* Corresponding author.
E-mail: mqin@aiofm.ac.cn (M. Qin).

https://doi.org/10.1016/j.jes.2021.09.005
1001-0742/

Introduction

As an important precursor of hydroxyl (OH) radicals, the photolysis of nitrous acid (HONO) contributes 25%–60% of primary production of atmospheric OH radicals (Elshorbany et al., 2009; Huang et al., 2017; Meng et al., 2020). Although atmospheric HONO has been studied for several decades, the sources of HONO remain considerable debated. Model-measurement discrepancies have been widely reported, and higher daytime HONO concentrations have been observed in remote, rural and urban regions compared to those predicted by the known reaction mechanisms (Hou et al., 2016; Lee et al., 2016; Li et al., 2012; Meusel et al., 2016; Michoud et al., 2014; Oswald et al., 2015; Sörgel et al., 2011a, 2011b; Tang et al., 2015; VandenBoer et al., 2013; Villena et al., 2011; Wang et al., 2017; Wong et al., 2013; Yang et al., 2014; Zhou et al., 2002), which has stimulated investigations of potential HONO formation mechanisms. Several mechanisms have been proposed based on field and laboratory studies, involving (i) the photosensitized reduction of NO_2 on organic substances, e.g., humic acids (George et al., 2005; Han et al., 2016; Scharko et al., 2017; Stemmler et al., 2006; Stemmler et al., 2007), (ii) the dynamic process of deposition of strong acid and rerelease of absorbed HONO from soil surfaces (VandenBoer et al., 2014a; VandenBoer et al., 2014b), (iii) the photolysis of surface HNO_3 and particulate nitrate (Ye et al., 2017; Ye et al., 2018; Ye et al., 2016; Zhou et al., 2003, 2011) and (iv) the biotic or abiotic production and release of nitrite in soil (Bhattarai et al., 2021; Donaldson et al., 2014; Oswald et al., 2013; Scharko et al., 2015; Su et al., 2011).

Several field studies have revealed high correlations between daytime HONO levels and the photolysis frequency $J(NO_2)$ or solar radiation and the NO_2 concentration, which points to an atmospheric HONO source involving the photosensitized reduction of NO_2 on organic substrates (Jiang et al., 2020; Kleffmann, 2007; Laufs et al., 2017; Ren et al., 2011; Sörgel et al., 2011a; Tsai et al., 2018). However, high daytime HONO fluxes of 2.84 nmol/(m^2•sec) and the maximum HONO concentration up to 20.64 ppbV were observed in an agricultural field in the North China Plain after fertilization, which may be attributed to biotic and abiotic HONO emissions from the soil (Tang et al., 2019; Xue et al., 2019). This formation mechanism has been proposed to be an effective HONO source in agricultural fields (Oswald et al., 2013; Su et al., 2011; Bhattarai et al., 2021), and it is closely related to NO emissions (Bhattarai et al., 2018; Mamtimin et al., 2016; Meusel et al., 2016; Weber et al., 2015), N_2O emissions (Maljanen et al., 2013), soil water content (Oswald et al., 2013; Weber et al., 2015; Wu et al., 2019) and fertilization (Tang et al., 2019, 2020; Xue et al., 2019, 2021).

Flux measurements provide direct information about the gas exchange processes between the surface and the atmosphere and are a better way to investigate the source of trace gases in the lower atmosphere. Several methods have been developed to measure land-atmosphere exchange of gas, which can be divided into direct micrometeorological methods (e.g., the eddy-covariance (EC) and disjunct eddy-covariance methods), indirect micrometeorological methods (e.g., the aerodynamic gradient (AG) method and the relaxed eddy-accumulation (REA) method) (Ren et al., 2011; Stella et al., 2012) and chamber methods (Tang et al., 2019, 2020; Xue et al., 2019). The micrometeorological methods allow larger spatial-scale measurements without influencing the underlying surface, whereas the chambers only represent small-scale spatial measurements. As the most common method, EC is widely used to study the land-atmosphere gas exchange. However, due to the lack of fast and sensitive EC-HONO measurement system, indirect methods such as the AG, REA and chamber methods have been applied to the field HONO flux measurements (Laufs et al., 2017; Ren et al., 2011; Zhou et al., 2011; Tang et al., 2020; Xue et al., 2019) and indicates the different HONO formation pathways. The photosensitized reaction of NO_2 on soil surfaces (Laufs et al., 2017), the photolysis of adsorbed HNO_3 (Zhang et al., 2012) and soil emissions (Tang et al., 2020; Xue et al., 2019) have been proposed as potential mechanisms for HONO production. Unfortunately, the few available HONO flux measurements, which are somewhat skewed to summertime periods despite the fact that the significance of HONO is likely higher in winter, limit the understanding and parameterization of surface HONO production and loss processes.

In this study, HONO flux measurements were performed over an agricultural field in winter in the Huaihe River Basin, which is an important grain production area in China, with grain output accounting for about 16% of the national total output. The arable area of the basin is about 12.7 million hectare, covering 12% of the total national arable area, and the application of nitrogen fertilizer accounts for 76.3% of the country (Cao et al., 2019). The heavy application of nitrogen fertilizers increases a potential to release HONO from agricultural soils, which affects the photochemistry, ozone and air quality in the Huaihe River Basin. Therefore, it is crucial to understand HONO formation pathways in agricultural fields. Here, we report HONO flux measurements over a winter-wheat field using the AG method coupled with the incoherent broadband cavity enhanced absorption spectrometer (IBBCEAS) technique. The unknown daytime HONO source was discussed based on the budget analysis and the origin of the surface HONO flux is investigated. The primary objective of our observations was to determine whether surface HONO fluxes are able to close the daytime HONO budget and to investigate whether the proposed HONO formation mechanisms dominate surface HONO flux at the studied agricultural field site.

1. Materials and methods

1.1. Site description

The measurements were performed over an agricultural field at the Shouxian National Climatological Observatory (32°25'47.8''N, 116°47'38.4''E), 9 km south of Shouxian, Anhui Province, China. The site is homogeneous farmland surrounded by a large amount of agricultural areas, with a low-traffic road located 250 m to the north. The agricultural field consists of 17 ha of rice-winter wheat rotation cropland which was fertilized, rotary tilled and sown before 31 October 2019,

with an ammonium-based fertilization amount of ~ 69 kg N/ha.

The HONO fluxes were measured from 14 December 2019 to 2 January 2020 during the growth of the winter wheat (from 0.07 to 0.08 m high). Before the measurements were conducted, rice was harvested before 18 October 2019. Thus, the surface was a mix of winter wheat seedling and sparse rice residuals. The mixing ratios of HONO and NO_2 at different heights were simultaneously measured using two IBBCEAS instruments with a time resolution of 1 min, which were placed in a thermostated container controlled by an air conditioner. The IBBCEAS technique is an optical technique that improves detection sensitivity by increasing the effective absorption optical path of the gas, which is explained in detailed elsewhere (Duan et al., 2018; Meng et al., 2020). The IBBCEAS instrument allows the detection of HONO down to 60 pptV (2σ) at 1 min time resolution and instrument showed excellent agreement with long path absorption photometer (LOPAP) (Duan et al., 2018). The light intensity was automatically calibrated every 1 hr throughout the campaign and the mirror reflectivity was calibrated weekly to ensure the accuracy and validity of the data.

1.2. Aerodynamic gradient and meteorological measurements

The HONO and NO_2 mixing ratios were measured at two heights above the canopy using a 3 m high gradient mast. The sampling inlets were mounted at heights of 0.15 and 1.5 m above the ground and positioned away from the mast to minimize the turbulence disruptions caused by the gradient mast (Fig. S1). Throughout the campaign, the sampling inlets were always above the wheat canopy, and the sample lines were heated with heating tape and were protected from radiation with black insulated tubing to avoid the condensation of water vapor and photolysis. Other trace gases, NO and O_3, were also measured during the campaign, which were measured using an NO_x analyzer (Model 42iTL, Thermo Scientific, USA) and an O_3 analyzer (Model 49i, Thermo Scientific, USA), respectively. The $PM_{2.5}$ concentrations were measured using a synchronized hybrid ambient real-time particulate (SHARP) Monitor (Model 5030, Thermo Scientific, USA).

Meteorological parameters included wind speed and direction (EL, Shanghai Meteorological Instrument Factory Co., China), air temperature (T_{air}) and relative humidity (RH) (HMP155, Vaisala, Finland) and solar radiation (BSRN3000, TRUWEL Instrument Inc., China) were measured continuously. The soil parameters such as soil temperature (T_{soil}) (TMC6-HC, ONSET, USA) and soil water content (θ) (S-SMD-M005, ONSET, USA) were also measured at different depths in the surface soil layer (5 and 10 cm). For the EC measurements, an integrated 3-D ultrasonic anemometer and open-path CO_2/H_2O analyzer (IRGASON, Campbell Sci. Inc., USA) was set 4 m above the ground, with data sampling and recording at 10 Hz. A footprint analysis with the ART Footprint Tool (Neftel et al. 2008) indicated that more than 80% of the field was in the EC mast footprint on average. Thus, at least 80% of the field was inside the gradient mast since it was below the EC mast.

1.3. Data treatment and AG flux uncertainty

The HONO flux was calculated at 30 min intervals by the AG method (as described in Section S1 of Appendix A. Supplementary data), which required a significant mixing ratio gradient across the height. The signal to noise ratio of the gradient, which is the ratio of the mean (ΔHONO) to the standard deviation (σ_{HONO}) of the HONO mixing ratio difference at two successive levels, can be used to evaluate whether the existence of a significant gradient difference in HONO mixing ratios between two measurement heights (Stella et al., 2012). The fluxes were calculated using only the significant gradient difference. Moreover, the data from instruments that were not simultaneously available (calibrations, intercomparisons and maintenance outage) and unusual conditions like dense fog events (e.g., 24 and 25 December 2019) were not considered in flux calculations. Finally, about 81% of the logged data was used to determine the HONO flux, and other measurements were also averaged for 30 min intervals for the subsequent flux analysis.

The uncertainty in the HONO flux ($\sigma_{F_{HONO}}$), which is directly related to the gradient error ($\sigma_{gradient}$) and the friction velocity (u_*) error (σ_{u_*}), is expressed as (Laufs et al., 2017):

$$\sigma_{F_{HONO}} = \sqrt{\sigma_{u_*}^2 + \sigma_{gradient}^2} \quad (1)$$

Since the HONO gradients were obtained by the IBBCEAS instruments at two heights, the quantification of the gradient strongly depended on the accuracy of the two instruments. Therefore, the IBBCEAS instruments were calibrated and intercompared several times throughout the field campaign. The external sampling inlets were placed adjacent to each other and identical sampling velocity was used to minimize the measurement deviations. The intercomparisons exhibited excellent agreement (HONO: R^2=0.987; NO_2: R^2=0.993), with slopes of close to 1 (HONO: 0.998 $\pm$ 0.020, NO_2: 0.992 $\pm$ 0.005) and small intercepts of 5 $\pm$ 13 (HONO) and 257 $\pm$ 57 pptV (NO_2), which demonstrates the credibility of the quantification of the HONO gradients (Fig. S2). Then, the errors of friction velocity (σ_{u_*}) and the gradient ($\sigma_{gradient}$) were calculated following the method of Laufs et al. (2017). The uncertainty of HONO flux was finally determined by Eq. (1), which was typically less than 35%.

2. Results and discussion

2.1. General observations

The meteorological parameters (global radiation, wind speed and direction, air temperature and relative humidity) and $PM_{2.5}$ are presented in Fig. S3. Cloudy days dominated the experimental periods, with the maximum global radiation only reaching 470 W/m^2, and clear sky only occurred on 22, 27, 28, 29 and 31 December, and the global radiation reached 562 W/m^2 at noontime. The daytime temperature was around 6°C and the relative humidity varied between 26% and 99%. The nighttime temperature ranged from −3.5 to 12.6°C and the relative humidity varied between 45% and 99%. During most of

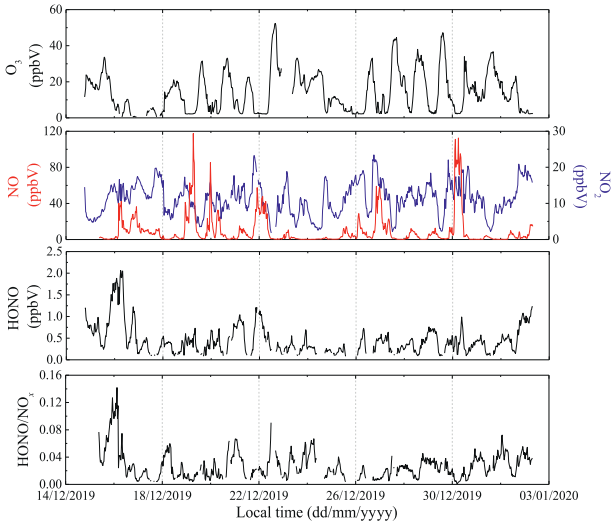

Fig. 1 – Time series of O_3, NO, NO_2 and HONO mixing ratios and HONO/NO_x ratio measured at 1.5 m height from 14 December 2019 to 2 January 2020.

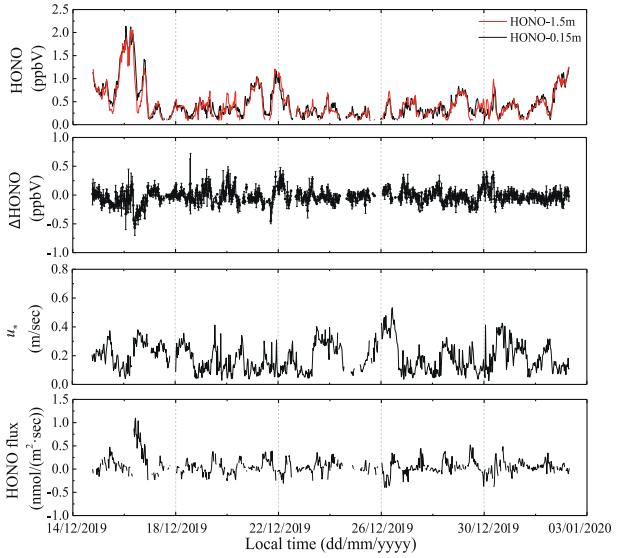

Fig. 2 – Time series of HONO mixing ratios measured at different heights (0.15 and 1.5 m), HONO mixing ratio differences between 1.5 and 0.15 m (△HONO), friction velocity (u_*) and HONO fluxes determined by the aerodynamic gradient (AG) method at geometric mean height z_{ref} = 0.38 m. The error bars denote the standard deviation.

the campaign, the prevailing winds were north and south sectors, with an average wind speed of 2.3 ± 1.4 m/sec. The $PM_{2.5}$ concentrations varied from 13 to 156 $\mu g/m^3$, with an average of 60 $\mu g/m^3$. The daily average $PM_{2.5}$ concentrations were below the Chinese National Ambient Air Quality Standard (Class II: 75 $\mu g/m^3$), except on 21, 23, 26 and 30 December when daily average $PM_{2.5}$ concentrations were above 80 $\mu g/m^3$.

The mixing ratios of O_3, NO, NO_2 and HONO exhibited diurnal and day-to-day variations (**Fig. 1**). During the measurement period, the O_3 mixing ratio varied from 0.52 to 52.35 ppbV, with a mean value of 14.30 ± 11.18 ppbV. The average mixing ratios of NO and NO_2 at 1.5 m were 9.23 ± 16.25 ppbV (0.08–117.53 ppbV) and 9.95 ± 4.20 ppbV (1.84–22.47 ppbV), respectively. The maximum NO mixing ratio up to 117.53 ppbV was observed at around 6:30 LT (local time) on December 19, which could be attributed to occasional local emissions from biomass burning and vehicles (NO/NO_x > 90%). Ambient HONO concentrations at 1.5 m height varied from below detection limits to 2.06 ppbV, with an average of 0.26 ± 0.24 ppbV during daytime (08:00-17:00 LT) and 0.52 ± 0.35 ppbV during nighttime (19:00-06:00 LT). The observed HONO levels are comparable to the levels measured in the rural areas of the Pearl River Delta (Backgarden, Guangzhou) (Li et al. 2012), but lower than those measured at a rural site (Wangdu, Hebei) in the North China Plain (Xue et al., 2020) and in polluted urban environments (Elshorbany et al., 2009; Hao et al., 2020; Huang et al., 2017; Jia et al., 2020; Li et al., 2018; Liu et al., 2020; Yu et al., 2009) as summarized in Table S1. The HONO/NO_x ratio varied from 0.1% to 14.2%, with an average of 2.7% ± 2.0%, which was lower than observations in other rural areas of China. The average HONO/NO_x ratio that exceed direct emissions (0.3%–1.3%) was observed (Kirchstetter et al., 1996; Kramer et al., 2020; Kurtenbach et al., 2001; Liang et al., 2017; Liu et al., 2017; Nakashima and Kajii, 2017), suggesting that ambient HONO levels were dominated by other sources rather than direct emissions in the agricultural field (Xue et al., 2020).

2.2. *Aerodynamic gradient HONO fluxes*

The HONO mixing ratios at 0.15 and 1.5 m levels, vertical mixing ratio differences (ΔHONO) and HONO fluxes are shown in **Fig. 2**. The HONO mixing ratio differences featured distinct diurnal patterns. The negative gradients during daytime indicate net emission and positive gradients at night indicate net deposition. The ΔHONO were up to −0.57 ppbV during daytime and 0.48 ppbV at night. The friction velocity u_* varied from 0.15 m/sec at night to 0.23 m/sec during daytime, with a maximum value up to 0.53 m/sec.

The calculated HONO fluxes ranged from −0.39 to 1.1 nmol/(m^2•sec), with an average of 0.06 ± 0.17 nmol/(m^2•sec), which was within the range of the HONO flux measurements in other suburban/rural/remote areas (−1.71–2.36 nmol/(m^2•sec)) (Harrison and Kitto, 1994; Laufs et al., 2017; Ren et al., 2011; Sörgel et al., 2015; Stutz et al., 2002; Tang et al., 2020; Xue et al., 2019; Zhang et al., 2012; Zhou et al., 2011). The observed HONO fluxes are comparable to the measurements in other agricultural fields (Laufs et al., 2017; Ren et al., 2011; Tang et al., 2020; Xue et al., 2019) and about an order of magnitude higher than for remote forest site (Table S2) (Ren et al., 2011; Sörgel et al., 2015), but are lower than the levels (–0.5–1.31 nmol/(m^2•sec)) measured at PROPHET site, which could be ascribed to differences in pH of canopy and soil surfaces between rural and forested sites (Sörgel et al., 2015; Zhang et al., 2012). The upward HONO fluxes were mostly observed throughout the whole campaign and the similar high emission event on 16 December was also observed at the PROPHET (Program for Research on Oxidants: Photochemistry, Emission and Transport) site (Zhang et al., 2012) and during

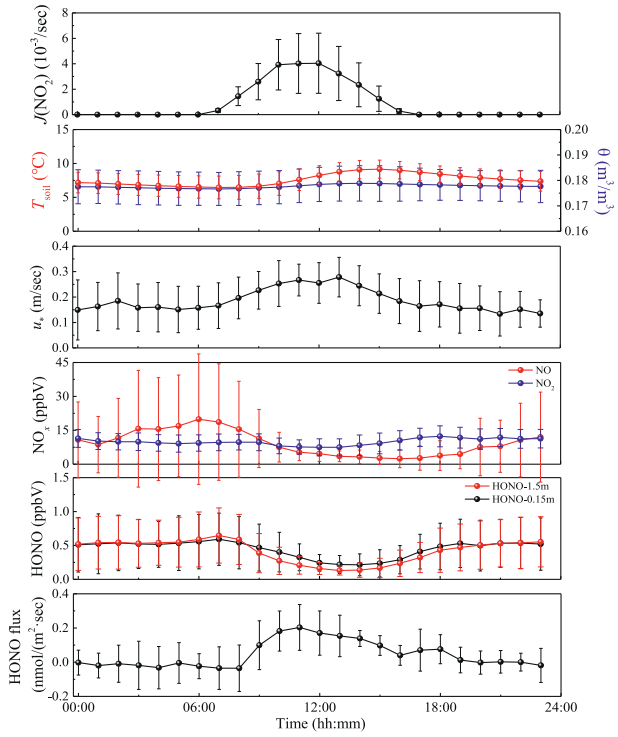

Fig. 3 – Diurnal profiles of HONO mixing ratio (0.15 and 1.5 m), HONO flux and its potential precursors and driving factors, i.e., NO, NO_2, photolysis frequency $J(NO_2)$, friction velocity (u_*), soil temperature (T_{soil}) and soil water content (θ) during the measurement period.

the PHOTONA 2 (PHOTOlytic sources of Nitrous Acid in the atmosphere) campaign (Laufs et al., 2017). The maximum HONO flux up to 1.1 nmol/(m^2•sec) is of the same order of magnitude as the REA HONO flux (maximum: 1.31 nmol/(m^2•sec)) (Zhang et al., 2012; Zhou et al., 2011) and the HONO flux (fertilized field: 1.51 nmol/(m^2•sec)) measured by the twin open-top chamber method (Xue et al., 2019).

2.3. *Diurnal variation of HONO flux*

The diurnal variations of meteorological parameters and chemical species are shown in **Fig. 3**. The HONO mixing ratio accumulated and remained relatively stable (~0.5 ppbV) at night, then gradually decreased after sunrise due to photolysis and vertical mixing, and reached the minimum value at noon. The significant daytime negative HONO gradients with higher HONO concentrations at 0.15 m indicate the existence of surface HONO source during the day. The diurnal NO profile exhibited a well-defined diurnal pattern with a morning concentration peak of 20 ppbV, followed by a decrease to the minimum during daytime. In contrast, the NO_2 exhibited a weak diurnal profile, with higher values of ~11 ppbV at night. The soil temperature and soil water content were also relatively stable with small variations, and an average T_{soil} of 7.59 ± 0.91°C and θ of 0.18 ± 0.001 m^3/m^3 were observed over the measurement period.

The high emission event (16 December 2019) was removed from the data since it did not represent a common flux profile in the agricultural field (Laufs et al., 2017). The diurnal profile of HONO flux generally followed the photolysis frequency $J(NO_2)$, with a maximum of 0.2 nmol/(m^2•sec) around noon. The upward HONO fluxes observed during the day imply the existence of a surface HONO source which is driven by solar radiation. In contrast, the nocturnal downward flux is close to zero (−0.003 ± 0.027 nmol/(m^2•sec)) was observed, indicating net deposition at night. The observed daytime HONO fluxes (−0.03 to 0.2 nmol/(m^2•sec)) are comparable to those measured by Laufs et al. (2017) (0.01−0.16 nmol/(m^2•sec)) and Tang et al. (2020) (−0.09−0.55 nmol/(m^2•sec)) in agricultural fields.

2.4. *Nocturnal HONO sources*

2.4.1. *Nocturnal homogeneous reaction*

The reaction of NO with OH is the most important homogeneous reaction for HONO formation. The net HONO production (P^{net}_{OH+NO}) at night is calculated as follows:

$$P^{net}_{OH+NO} = k_{OH+NO}[OH][NO] - k_{OH+HONO}[OH][HONO] \quad (2)$$

The rate constants of k_{OH+NO} and $k_{OH+HONO}$ are 9.8 × 10^{-12} and 6.0 × 10^{-12} cm^3/(molecules•sec), respectively (Atkinson et al., 2004, 2005), and [NO] and [HONO] are hourly average mixing ratios of NO and HONO, respectively. The nocturnal OH radical concentration ([OH]) was estimated since it was not available during the campaign. The average OH concentration of 5 × 10^5 molecules/cm^3 was observed at night in summer in rural environments (Tan et al., 2017), and the ratio of $[OH]_{summer}/[OH]_{winter}$ is about 2 (Spataro et al., 2013; Zhang et al., 2019). Therefore, the nocturnal OH concentration of 2.5 × 10^5 molecules/cm^3 was used in this study, which was comparable to the OH levels observed in winter in Beijing (Ma et al., 2019; Tan et al., 2018).

The nocturnal variations of P^{net}_{OH+NO}, NO and HONO are illustrated in **Fig. 4**. The P^{net}_{OH+NO} ranged from 0.04 to 0.15 ppbV/hr, with an average of 0.09 ppbV/hr, which increased before midnight and remained relatively constant after midnight. The profile of P^{net}_{OH+NO} approximately followed that of NO due to the higher NO levels (11.13 ppbV) compared to HONO levels (0.53 ppbV) governing the variation of P^{net}_{OH+NO}. Considering ±50% uncertainty of OH values to estimate P^{net}_{OH+NO}, the P^{net}_{OH+NO} varied from 0.02 (0.06) to 0.07 (0.21) ppbV/hr for −50% (+50%) variations of OH concentration. The levels of P^{net}_{OH+NO} are comparable to those measured at a rural site (Li et al., 2012) but lower than those measured in polluted urban areas (Hao et al., 2020; Zhang et al., 2019). By integrating P^{net}_{OH+NO} before midnight (19:00-00:00 LT) when HONO mixing ratios increased, the accumulated amount of HONO from homogeneous reaction was 0.18−0.54 ppbV for ±50% variations of OH concentration, which can explain the HONO production (0.08 ppbV) in the first half of the night.

2.4.2. *Heterogeneous conversion of NO_2*

The heterogeneous reaction of NO_2 on the surface are considered as an important pathway for nocturnal HONO formation as reported in laboratory and field studies (Cui et al., 2018; Finlayson-Pitts et al., 2003; Hao et al., 2020; Meng et al., 2020).

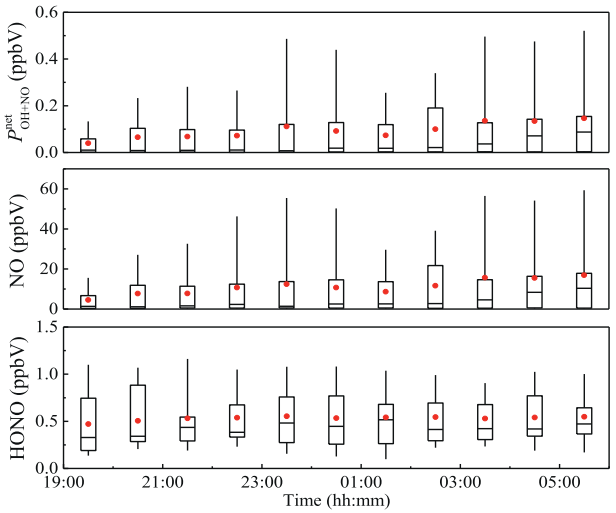

Fig. 4 – Nocturnal hourly average net HONO production (P^{net}_{OH+NO}), NO and HONO. The boxes represent 25% to 75% of the data, and the whiskers 90% of data. The red circle and black line refer to the mean and median of data, respectively.

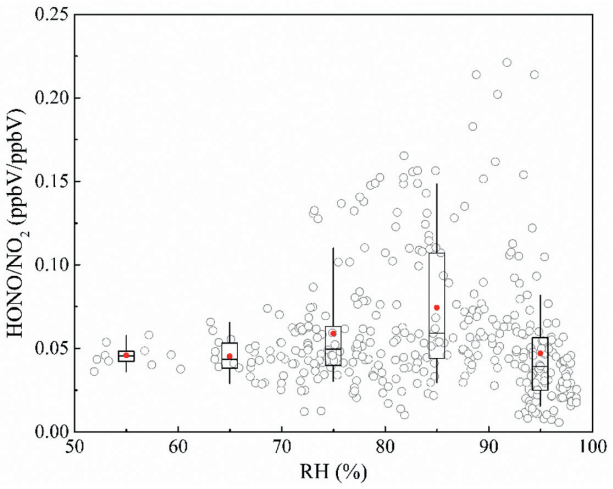

Fig. 5 – Scatter plot of the HONO/NO_2 against RH for the height near the surface (0.15 m) at night. The mean (red circle), median (black line), boxes represent 25% to 75% of data and whisker represent 10% to 90% of data are shown in each bin of relative humidity (RH).

During the measurement period, the nocturnal HONO/NO_2 ratios ranged from 0.4% to 18.4% at the lower level and from 0.4% to 15.3% at the upper levels, with an average of 5.4% and 4.6%, respectively, which was comparable to the values reported in previous studies (Hao et al., 2020; Huang et al., 2017; Su et al., 2008). The higher HONO/NO_2 ratios close to the surface implied that nocturnal HONO was formed and released near the ground. However, aerosol surface, as another important heterogeneous reaction medium, also influences the heterogeneous conversion of NO_2 (Cui et al., 2018; Meng et al., 2020; Zhang et al., 2020). Since the aerosol surface area was not measured in the present study, $PM_{2.5}$ concentrations were used as an alternative to identify the impact of aerosols. The weak anti-correlation of HONO/NO_2 ratio with $PM_{2.5}$ concentration (Fig. S4) suggested that heterogeneous HONO production on aerosol surfaces could be negligible.

The surface-adsorbed water is also a factor influencing NO_2 hydrolysis on wet surface (Finlayson-Pitts et al., 2003; Stutz et al., 2004), however, the exact mechanisms are still unclear. The influence of RH on heterogeneous HONO formation is investigated in this study, as illustrated in **Fig. 5**. The HONO/NO_2 ratio increased along with RH when RH increased from 55% to 85% and then decreased with the further increase of RH, which was in agreement with previous studies (Huang et al., 2017; Li et al., 2012; Liu et al., 2019). The negative dependency of HONO/NO_2 ratio on RH was found when RH was above 85%, which could be attributed to the rapid growth in the number of water mono-layers leading to the less reactive to NO_2 and the effective uptake of HONO on saturated surface (Cui et al., 2018; Li et al., 2012; Liu et al., 2019).

The NO_2–to–HONO conversion rate (C_{HONO}) is generally used to evaluate the efficiency of heterogeneous conversion of NO_2, which is calculated from Eq. (3) by assuming that the observed nocturnal HONO comes from the NO_2 heterogeneous reaction (Su et al., 2008).

$$C_{HONO} = \frac{\frac{[HONO]_{t_2}}{[NO_2]_{t_2}} - \frac{[HONO]_{t_1}}{[NO_2]_{t_1}}}{t_2 - t_1} \quad (3)$$

where $[HONO]_t$ and $[NO_2]_t$ represent the HONO and NO_2 mixing ratios at the measuring time t, and the fitted slope of HONO/NO_2 against time is taken as the NO_2–to–HONO conversion rate (Liu et al., 2019). The nocturnal C_{HONO} ranged from 0.002 to 0.015 hr at 0.15 m and 0.002 to 0.008 hr at 1.5 m, with an average value of 0.008 ± 0.004 and 0.005 ± 0.002 hr, respectively. The higher C_{HONO} near the surface also supports that the ground surface is the predominant surface where nocturnal HONO is formed (Kleffmma et al., 2003; VandenBoer et al., 2013). The derived C_{HONO} in this study are lower than those observed by Su et al. (2008) (0.016 ± 0.014 hr) and Li et al. (2012) (0.016 ± 0.014 hr) in rural areas of the Pearl River Delta and by Alicke et al. (2003) at a rural site in Pabsthum (0.018 ± 0.009 hr), but comparable to the observations in rural forested region in Bavaria (0.0075 ± 0.0045 hr, Sörgel et al., 2011b) and urban environments (Huang et al., 2017; Liu et al., 2019; Wang et al., 2013; Wang et al., 2017).

2.5. *Daytime HONO sources*

2.5.1. *Missing daytime HONO source*

The daytime HONO budget analysis (Eq. (4)) is applied to investigate the unknown HONO source and identify whether the surface HONO flux can explain the unknown HONO source. The lower-level data were used for the HONO budget analysis since they described the ground source processes better (Laufs et al., 2017). However, the NO data were only measured at 1.5 m height throughout the campaign, which was used

here.

$$\frac{\mathrm{dHONO}}{\mathrm{dt}} = (P_{\mathrm{OH+NO}} + P_{\mathrm{unknown}}) - (L_{\mathrm{OH+HONO}} + L_{\mathrm{photo}}) \pm T_{\mathrm{v}} \pm T_{\mathrm{h}} \quad (4)$$

The production/loss terms of HONO contain homogeneous reaction (P_{OH+NO}), unknown HONO source ($P_{unknown}$), reaction of OH with HONO ($L_{OH+HONO}$) and photolysis (L_{photo}). The terms of T_v and T_h describe the vertical and horizontal transport processes, which are negligible due to rapid photolysis and relatively homogeneous atmosphere (Dillon et al., 2002; Li et al., 2018; Liu et al., 2019; Sörgel et al., 2011a).

Simplifying Eq. (4), the unknown daytime HONO source can be derived by Eq. (5), where the dHONO/dt is approximated by $\triangle$HONO/$\triangle$t. The daytime OH concentration was calculated by the empirical equation (Eq. (6)), which was based on the strong correlations of OH concentration with photolysis frequency $J(O^1D)$ (Liu et al., 2019; Rohrer and Berresheim, 2006). The calculated OH concentration ranged from 3.3×10^6 to 4.6×10^6 molecules/cm^3 at noontime, which was comparable to observations over northern China in winter (Tan et al., 2018).

$$P_{\mathrm{unknown}} = k_{\mathrm{OH+HONO}}[\mathrm{OH}][\mathrm{HONO}] + J(\mathrm{HONO})[\mathrm{HONO}] + \frac{\triangle\,\mathrm{HONO}}{\triangle\,t} - k_{\mathrm{OH+NO}}[\mathrm{OH}][\mathrm{NO}] \quad (5)$$

$$[\mathrm{OH}] = a \times \left(J\left(\mathrm{O^1D}\right)/10^{-5}\right)^b + c \quad (6)$$

where J(HONO) is photolysis frequency of HONO, and a, b and c characterize the average influence of the chemical environment on OH radical at a specific research site. Coefficients $a = 4.2 \times 10^6$ molecules/cm^3 and b=1 reflects the average influence of reactants on OH at the research site and the combined effects of all photolytic processes (e.g. photolysis of O_3, NO_2, HCHO, H_2O_2 and HONO), respectively. The coefficient c counts the light-independent processes which is 0.2×10^6 molecules/cm^3 in winter.

The average diurnal HONO production/loss rates and HONO flux rate from 8:00 to 17:00 LT are presented in **Fig. 6**. Surface HONO fluxes were converted into column HONO production rate by dividing them by the surface layer height which was assumed to be homogeneously mixed (Tsai et al., 2018; Su et al., 2011). The photodecomposition (L_{photo}) dominated the daytime HONO loss, with an average of 0.65 ppbV/hr around noon (11:00–14:00 LT), and $L_{OH+HONO}$ was very small and less than 3% of L_{photo}. The average noontime $P_{unknown}$ of 0.35 ppbV/hr was comparable to the P_{OH+NO} (0.28 ppbV/hr), which contributed about 55% of daytime HONO productivity. The derived $P_{unknown}$ is comparable to observations by Zhou et al. (2002) in rural areas of New York State (0.22 ppbV/hr) and by Kleffmann et al. (2005) at a forest site near Jülich (0.55 ppbV/hr), but smaller than those reported by Li et al. (2012) in the polluted rural environments of the Pearl River Delta (0.77 ppbV/hr), Jia et al. (2020) in the urban atmosphere of Beijing (2.33 ppbV/hr) and Liu et al. (2019) at a suburban site of Nanjing (1.04 ppbV/hr). The average HONO flux rate (P_{flux}) of 0.08 ppbV/hr was derived at noontime, which is comparable to the values reported by Tang et al. (2020) at the same site (0.06 ppbV/hr) and Xue et al. (2019) in a rural area of the North China Plain (0.07 ppbV/hr), and accounted for ~23% of the unknown daytime HONO source. However, when the mixing layer height of 70 m was adopted at noontime according to Xue et al. (2021), the unknown HONO source could be explained by the P_{flux} (0.30 ppbV/hr). And almost all of the HONO production (92%) could be explained by the P_{OH+NO} and surface HONO flux, which is in agreement with the results reported by Xue et al. (2021). Therefore, the knowledge of boundary layer processes is crucial for further studies, which influences the understanding of atmospheric HONO sources and sinks.

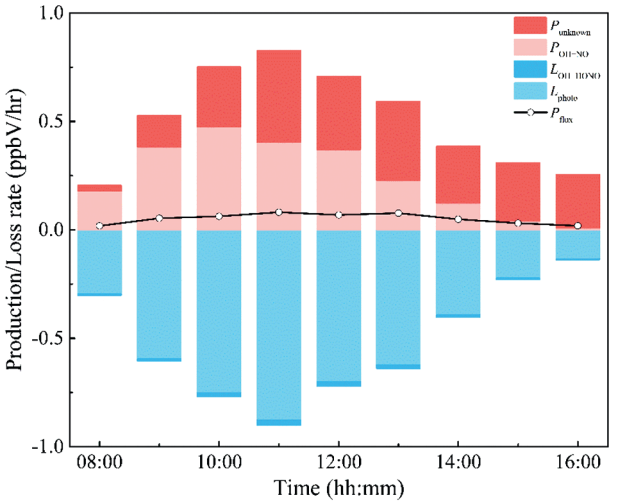

Fig. 6 – Average daytime HONO production ($P_{unknown}$: unknown HONO source strength; P_{OH+NO}: homogeneous reaction rate) and loss ($L_{OH+HONO}$: reaction rate of OH with HONO; L_{photo}: photolysis rate) rates and HONO flux rate (P_{flux}) in winter in agricultural fields.

Table 1 – Correlation coefficients (R^2) between average diurnal HONO flux (08:00–17:00 LT (local time)) and different variables. The bold numbers denote the strong correlations observed during the field campaign.

	Diurnal average HONO fluxes
T_{soil}	0.018
θ	0.0001
T_{air}	0.042
NO	0.035
$J(NO_2)$	**0.925**
NO_2	**0.763**
$J(NO_2) \times NO_2$	**0.840**

T_{soil}: soil temperature; θ: soil water content; T_{air}: air temperature; NO: NO concentration; NO_2: NO_2 concentration; $J(NO_2)$: photolysis frequency of NO_2; $J(NO_2) \times NO_2$: the product of the photolysis frequency $J(NO_2)$ and NO_2 concentration.

2.5.2. *Potential surface sources for HONO flux*

The upward HONO flux indicates the existence of surface HONO source during daytime. To investigate the origin of the surface HONO flux, the correlations between diurnal HONO fluxes and potential precursors and controlling parameters were analyzed (**Table 1**). Strong positive correlations of the HONO flux with the photolysis frequency $J(NO_2)$ ($R^2 = 0.925$)

and the product of $J(NO_2) \times NO_2$ ($R^2 = 0.840$) were observed during the day, suggesting a light-driven daytime HONO source, possibly via NO_2 conversion as proposed by laboratory studies (George et al., 2005; Han et al., 2016; Stemmler et al., 2006). Similar correlations between the HONO flux and the solar radiation $\times$ NO_2 or $J(NO_2) \times NO_2$ were also observed by Ren et al. (2011) and Laufs et al. (2017), who found that the daytime HONO fluxes were well correlated with the products of the NO_2 concentrations and solar radiation/$J(NO_2)$ in agricultural fields. However, strong correlations between daytime HONO flux and both solar radiation $\times$ NO_2 ($R^2 = 0.58$) and $HNO_3 \times$ UV solar radiation ($R^2 = 0.66$) were also observed in rural areas during the UBWOS 2012 (Uintah Basin Wintertime Ozone Study) campaign (Tsai et al., 2018). Unfortunately, the lack of surface nitrate measurements in this study makes it impossible to evaluate the influences of the HNO_3 photolysis mechanism (Zhang et al., 2012; Zhou et al., 2011). In addition, a very weak correlation was observed between the HONO flux and $J(NO_2) \times NO_2$ above a forest canopy, which could be caused by the influence of the canopy. The surface processes may be decoupled from the air above the forest canopy when measurements are made above high trees.

Another potential HONO source, HONO release from soil by biotic and/or abiotic processes proposed by Su et al. (2011) and Oswald et al. (2013), could depend strongly on the soil water content and temperature, and would be expected to be associated with the NO flux (Bargsten et al., 2010). To investigate the soil HONO emissions, the HONO and NO_x fluxes were measured simultaneously by applying the automatic chamber method in the agricultural field. The daytime HONO flux was correlated with NO flux ($R = 0.64$), and the HONO flux from the fresh soil samples were found to be of the same order of magnitude as the field measurements, indicating the HONO emissions from agricultural soil (Tang et al., 2020). However, the weak correlations of HONO flux with soil temperature, soil water content and NO concentration were observed in this study (Table 1), implying that soil HONO emission played a minor role. The positive intercept (0.025 ± 0.019 nmol/(m^2•sec)) of the correlation plots of HONO flux and $J(NO_2) \times NO_2$ (Fig. S5) may reveal the magnitude of the soil HONO emissions and/or other light-independent HONO sources. However, compared to the measured HONO fluxes, the small intercept indicates that the light-independent HONO sources are of minor importance during the day. Furthermore, the nitrification and denitrification processes, like most biological reactions, are strongly influenced by soil temperature and cease when the soil temperature is below 5°C (Western Plant Health Association, 2002). The average soil temperature of 7°C was observed in this study, which was cold enough to weaken biological reactions. Thus, we believe that soil HONO emissions are of minor importance in this field campaign, which is in agreement with previous field studies in which soil HONO emissions were found to be insignificant and the daytime HONO source was well correlated with the solar radiation (Oswald et al., 2015; Tsai et al., 2018). Finally, two possible physicochemical and/or biological processes could account for the differences in the observations: (i) the average temperature was about 5°C lower than that observed by Tang et al. (2020), which could reduce nitrite production from microbiological processes, and/or (ii) the soil HONO emissions may be decreasing after the initial fertilization period (Bhattarai et al., 2019; Xue et al., 2021), the lower daytime HONO fluxes were observed in this campaign compared to those observed by Tang et al. (2020), which were measured shortly after fertilization.

3. Conclusions

The HONO mixing ratios and fluxes were measured in the Huaihe River Basin from 14 December 2019 to 2 January 2020 by applying the aerodynamic gradient method coupled with the IBBCEAS technique. Ambient HONO concentrations ranged from below detection limits to 2.06 ppbV, which were comparable to the HONO levels measured in rural areas but lower than measurements in the polluted urban environments. The average HONO flux was 0.06 ± 0.17 nmol/(m^2•sec), indicating that the agricultural field was a net HONO source for the overlying atmosphere. The upward HONO fluxes were mostly observed during the day, and the diurnal profile of HONO flux approximately followed the variation of solar radiation, which corresponded to a photolytically driven surface HONO source. Deposition was dominant at night, with a small negative HONO flux of -0.003 ± 0.027 nmol/(m^2•sec).

The higher HONO/NO_2 ratio and NO_2–to–HONO conversion rate close to the surface suggested that nocturnal HONO production was dominated by heterogeneous NO_2 conversion on the ground surface. The daytime HONO budget analysis was utilized to determine the unknown HONO source. The average strength of the unknown HONO source was 0.35 ppbV/hr at noontime, which contributed about 55% of the daytime HONO productivity. The derived noontime HONO flux rate of 0.08 ppbV/hr was comparable to the values reported in other rural areas of China, which accounted for ~23% of the unknown daytime HONO source. Significant correlations of the HONO flux with the photolysis frequency $J(NO_2)$ and the product of $J(NO_2) \times NO_2$ were observed for the daytime hours, suggesting a light-driven HONO source responsible for the surface HONO flux during the day. However, it is challenging to explicitly determine the mechanism of surface HONO source due to the limited measurement and dominating correlation of most mechanisms with solar radiation. To better understand the surface HONO flux and precise mechanisms, more comprehensive measurements are needed, including better characterization of the surface chemical composition and profound knowledge of boundary layer processes. The AG method together with the IBBCEAS technique provides a useful flux measurement technique, which will be applied in future field studies.

Acknowledgments

This work was supported by the National Natural Science Foundation of China (Nos. 41875154, U19A2044 and 91544104) and the Anhui Provincial Key R&D Program (No. 202104i07020010). We gratefully acknowledge the Shouxian National Climatology Observatory for providing the observation site and relevant auxiliary data.

Appendix A Supplementary data

Supplementary material associated with this article can be found in the online version at doi:10.1016/j.jes.2021.09.005.

REFERENCES

Alicke, B., Geyer, A., Hofzumahaus, A., Holland, F., Konrad, S., Pätz, H.W., et al., 2003. OH formation by HONO photolysis during the BERLIOZ experiment. J. Geophys. Res. 108, 8247.

Atkinson, R., Baulch, D.L., Cox, R.A., Crowley, J.N., Hampson, J.R.F., Hynes, R.G., et al., 2004. Evaluated kinetic and photochemical data for atmospheric chemistry: volume I–Gas phase reactions of O_x,HO_x,NO_x and SO_x species. Atmos. Chem. Phys. 4, 1461–1738.

Atkinson, R., Baulch, D.L., Cox, R.A., Crowley, J.N., Hampson, J.R.F., Hynes, R.G., et al. 2005. Summary of evaluated kinetic and photochemical data for atmospheric chemistry. IUPAC Subcomm on Gas Kinet Data Eval for Atmos Chem. N. C. Park: Research Triangle.

Bargsten, A., Falge, E., Pritsch, K., Huwe, B., Meixner, F.X., 2010. Laboratory measurements of nitric oxide release from forest soil with a thick organic layer under different understory types. Biogeosciences 7, 1425–1441.

Bhattarai, H.R., Liimatainen, M., Nykänen, H., Kivimäenpää, M., Martikainen, P.J., Maljanen, M., 2019. Germinating wheat promotes the emission of atmospherically significant nitrous acid (HONO) gas from soils. Soil Biol. Biochem. 136, 107518.

Bhattarai, H.R., Virkajärvi, P., Yli-Pirilä, P., Maljanen, M., 2018. Emissions of atmospherically important nitrous acid (HONO) gas from northern grassland soil increases in the presence of nitrite (NO2-). Agric. Ecosyst. Environ. 256, 194–199.

Bhattarai, H.R., Wanek, W., Siljanen, H.M.P., Ronkainen, J.G., Liimatainen, M., Hu, Y., et al., 2021. Denitrification is the major nitrous acid production pathway in boreal agricultural soils. Commun. Earth Environ. 2, 54.

Cao, Q., Hao, Z., Yuan, F., Berndtsson, R., Xu, S., Gao, H., et al., 2019. On the predictability of daily rainfall during rainy season over the Huaihe River Basin. Water 11, 916.

Cui, L., Li, R., Zhang, Y., Meng, Y., Fu, H., Chen, J., 2018. An observational study of nitrous acid (HONO) in Shanghai, China: the aerosol impact on HONO formation during the haze episodes. Sci. Total Environ. 630, 1057–1070.

Dillon, M.B., Lamanna, M.S., Schade, G.W., Goldstein, A.H., Cohen, R.C., 2002. Chemical evolution of the Sacramento urban plume: transport and oxidation. J. Geophys. Res.-Atmos. 107 ACH 3-1–ACH 3-15.

Donaldson, M.A., Bish, D.L., Raff, J.D., 2014. Soil surface acidity plays a determining role in the atmospheric-terrestrial exchange of nitrous acid. Proc. Natl. Acad. Sci. USA 111, 18472–18477.

Duan, J., Qin, M., Ouyang, B., Fang, W., Li, X., Lu, K., et al., 2018. Development of an incoherent broadband cavity-enhanced absorption spectrometer for in situ measurements of HONO and NO_2. Atmos. Meas. Tech. 11, 4531–4543.

Elshorbany, Y.F., Kleffmann, J., Kurtenbach, R., Rubio, M., Lissi, E., Villena, G., et al., 2009. Summertime photochemical ozone formation in Santiago, Chile. Atmos. Environ. 43, 6398–6407.

Finlayson-Pitts, B.J., Wingen, L.M., Sumner, A.L., Syomin, D., Ramazan, K., 2003. The heterogeneous hydrolysis of NO_2 in laboratory systems and in outdoor and indoor atmospheres: an integrated mechanism. Phys. Chem. Chem. Phys. 5, 223–242.

George, C., Strekowski, R.S., Kleffmann, J., Stemmler, K., Ammann, M., 2005. Photoenhanced uptake of gaseous NO_2 on solid organic compounds: a photochemical source of HONO? Faraday Discuss. 130, 195–210.

Hao, Q., Jiang, N., Zhang, R., Yang, L., Li, S., 2020. Characteristics, sources, and reactions of nitrous acid during winter at an urban site in the Central Plains Economic Region in China. Atmos. Chem. Phys. 20, 7087–7102.

Harrison, R.M., Kitto, A.-M. N., 1994. Evidence for a surface source of atmospheric nitrous acid. Atmos. Environ. 28, 1089–1094.

Han, C., Yang, W., Wu, Q., Yang, H., Xue, X., 2016. Heterogeneous photochemical conversion of NO_2 to HONO on the humic acid surface under simulated sunlight. Environ. Sci. Technol. 50, 5017–5023.

Hou, S., Tong, S., Ge, M., An, J., 2016. Comparison of atmospheric nitrous acid during severe haze and clean periods in Beijing. China. Atmos. Environ. 124, 199–206.

Huang, R., Yang, L., Cao, J., Wang, Q., Tie, X., Ho, K., et al., 2017. Concentration and sources of atmospheric nitrous acid (HONO) at an urban site in Western China. Sci. Total Environ. 593-594, 165–172.

Jia, C., Tong, S., Zhang, W., Zhang, X., Li, W., Wang, Z., et al., 2020. Pollution characteristics and potential sources of nitrous acid (HONO) in early autumn 2018 of Beijing. Sci. Total Environ. 735, 139317.

Jiang, Y., Xue, L., Gu, R., Jia, M., Zhang, Y., 2020. Sources of nitrous acid (HONO) in the upper boundary layer and lower free troposphere of the North China Plain: insights from the Mount Tai Observatory. Atmos. Chem. Phys. 20, 12115–12131.

Kirchstetter, T.W., Harley, R.A., Littlejohn, D., 1996. Measurement of nitrous acid in motor vehicle exhaust. Environ. Sci. Technol. 30, 2843–2849.

Kleffmann, J., 2007. Daytime sources of nitrous acid (HONO) in the atmospheric boundary layer. ChemPhysChem 8, 1137–1144.

Kleffmann, J., Gavriloaiei, T., Hofzumahaus, A., Holland, F., Koppmann, R., Rupp, L., et al., 2005. Daytime formation of nitrous acid: a major source of OH radicals in a forest. Geophys. Res. Lett. 32 L05818.

Kleffmann, J., Kurtenbach, R., Lörzer, J., Wiesen, P., Kalthoff, N., Vogel, B., et al., 2003. Measured and simulated vertical profiles of nitrous acid part I: field measurements. Atmos. Environ. 37, 2949–2955.

Kramer, L.J., Crilley, L.R., Adams, T.J., Ball, S.M., Pope, F.D., Bloss, W.J., 2020. Nitrous acid (HONO) emissions under real-world driving conditions from vehicles in a UK road tunnel. Atmos. Chem. Phys. 20, 5231–5248.

Kurtenbach, R., Becker, K.H., Gomes, J.A.G., Kleffmann, J., Lörzer, J.C., Spottler, M., et al., 2001. Investigations of emissions and heterogeneous formation of HONO in a road traffic tunnel. Atmos. Environ. 35, 3385–3394.

Laufs, S., Cazaunau, M., Stella, P., Kurtenbach, R., Cellier, P., Mellouki, A., et al., 2017. Diurnal fluxes of HONO above a crop rotation. Atmos. Chem. Phys. 17, 6907–6923.

Lee, J.D., Whalley, L.K., Heard, D.E., Stone, D., Dunmore, R.E., Hamilton, J.F., et al., 2016. Detailed budget analysis of HONO in central London reveals a missing daytime source. Atmos. Chem. Phys. 16, 2747–2764.

Li, D., Xue, L., Wen, L., Wang, X., Chen, T., Mellouki, A., et al., 2018. Characteristics and sources of nitrous acid in an urban atmosphere of northern China: results from 1-yr continuous observations. Atmos. Environ. 182, 296–306.

Li, X., Brauers, T., Häseler, R., Bohn, B., Fuchs, H., Hofzumahaus, A., et al., 2012. Exploring the atmospheric chemistry of nitrous acid (HONO) at a rural site in Southern China. Atmo. Chem. Phys. 12, 1497–1513.

Liang, Y., Zha, Q., Wang, W., Cui, L., Lui, K.H., Ho, F.H., et al., 2017. Revisiting nitrous acid (HONO) emission from onroad vehicles: a tunnel study with a mixed fleet. J. Air Waste Manag. 67, 797–805.

Liu, Y., Lu, K., Ma, y., Yang, X., Zhang, W., Wu, Y., et al., 2017. Direct emission of nitrous acid (HONO) from gasoline cars in China

determined by vehicle chassis dynamometer experiments. Atmos. Environ. 169, 89–96.
Liu, Y., Ni, S., Jiang, T., Xing, S., Zhang, Y., Bao, X., et al., 2020. Influence of Chinese New Year overlapping COVID-19 lockdown on HONO sources in Shijiazhuang. Sci. Total Environ. 745, 141025.
Liu, Y., Nie, W., Xu, Z., Wang, T., Wang, R., Li, Y., et al., 2019. Semi-quantitative understanding of source contribution to nitrous acid (HONO) based on 1 year of continuous observation at the SORPES station in eastern China. Atmos. Chem. Phys. 19, 13289–13308.
Ma, X., Tan, Z, Lu, K, Yang, X, Liu, Y, Li, S., et al., 2019. Winter photochemistry in Beijing: observation and model simulation of OH and HO_2 radicals at an urban site. Sci. Total Environ. 685, 85–95.
Maljanen, M., Yli-Pirilä, P., Hytönen, J., Joutsensaari, J., Martikainen, P.J., 2013. Acidic northern soils as sources of atmospheric nitrous acid (HONO). Soil Biol. Biochem. 67, 94–97.
Mamtimin, B., Meixner, F.X., Behrendt, T., Badawy, M., Wagner, T., 2016. The contribution of soil biogenic NO and HONO emissions from a managed hyperarid ecosystem to the regional NO_x emissions during growing season. Atmos. Chem. Phys. 16, 10175–10194.
Meusel, H., Kuhn, U., Reiffs, A., Mallik, C., Harder, H., Martinez, M., et al., 2016. Daytime formation of nitrous acid at a coastal remote site in Cyprus indicating a common ground source of atmospheric HONO and NO. Atmos. Chem. Phys. 16, 14475–14493.
Meng, F., Qin, M., Tang, K., Duan, J., Fang, W., Liang, S., et al., 2020. High-resolution vertical distribution and sources of HONO and NO_2 in the nocturnal boundary layer in urban Beijing, China. Atmos. Chem. Phys. 20, 5071–5092.
Michoud, V., Colomb, A., Borbon, A., Miet, K., Beekmann, M., Camredon, M., et al., 2014. Study of the unknown HONO daytime source at a European suburban site during the MEGAPOLI summer and winter field campaigns. Atmos. Chem. Phys. 14, 2805–2822.
Nakashima, Y., Kajii, Y., 2017. Determination of nitrous acid emission factors from a gasoline vehicle using a chassis dynamometer combined with incoherent broadband cavity-enhanced absorption spectroscopy. Atmos. Environ. 575, 287–293.
Neftel, A., Spirig, C., Ammann, C., 2008. Application and test of a simple tool for operational footprint evaluations. Environ. Pollut. 152, 644–652.
Oswald, R., Behrendt, T., Ermel, M., Wu, D., Su, H., Cheng, Y., et al., 2013. HONO emissions from soil bacteria as a major source of atmospheric reactive nitrogen. Science 341, 1233–1235.
Oswald, R., Ermel, M., Hens, K., Novelli, A., Ouwersloot, H.G., Paasonen, P., et al., 2015. A comparison of HONO budgets for two measurement heights at a field station within the boreal forest in Finland. Atmos. Chem. Phys. 15, 799–813.
Ren, X., Sanders, J.E., Rajendran, A., Weber, R.J., Goldstein, A.H., Pusede, S.E., et al., 2011. A relaxed eddy accumulation system for measuring vertical fluxes of nitrous acid. Atmos. Meas. Tech. 4, 2093–2103.
Rohrer, F., Berresheim, H., 2006. Strong correlation between levels of tropospheric hydroxyl radicals and solar ultraviolet radiation. Nature 442, 184–187.
Scharko, N.K., Martin, E.T., Losovyj, Y., Peters, D.G., Raff, J.D., 2017. Evidence for quinone redox chemistry mediating daytime and nighttime NO_2-to-HONO conversion on soil surfaces. Environ. Sci. Technol. 51, 9633–9643.
Scharko, N.K., Schutte, U.M., Berke, A.E., Banina, L., Peel, H.R., Donaldson, M.A., et al., 2015. Combined flux chamber and genomics approach links nitrous acid emissions to ammonia oxidizing bacteria and archaea in urban and agricultural soil. Environ. Sci. Technol. 49, 13825–13834.
Spatato, F., Ianniello, A., Esposito, G., Allegrini, I., Zhu, T., Hu, M., 2013. Occurrence of atmospheric nitrous acid in the urban area of Beijing (China). Sci. Total Environ. 447, 210–224.
Sörgel, M., Regelin, E., Bozem, H., Diesch, J.M., Drewnick, F., Fischer, H., et al., 2011a. Quantification of the unknown HONO daytime source and its relation to NO_2. Atmos. Chem. Phys. 11, 10433–10447.
Sörgel, M., Trebs, I., Serafimovich, A., Moravek, A., Held, A., Zetzsch, C., 2011b. Simultaneous HONO measurements in and above a forest canopy: influence of turbulent exchange on mixing ratio differences. Atmos. Chem. Phys. 11, 841–855.
Sörgel, M., Trebs, I., Wu, D., Held, A., 2015. A comparison of measured HONO uptake and release with calculated source strengths in a heterogeneous forest environment. Atmos. Chem. Phys. 15, 9237–9251.
Stella, P., Loubet, B., Laville, P., Lamaud, E., Cazaunau, M., Laufs, S., et al., 2012. Comparison of methods for the determination of NO-O_3-NO_2 fluxes and chemical interactions over a bare soil. Atmos. Meas. Tech. 5, 1241–1257.
Stemmler, K., Ammann, M., Donders, C., Kleffmann, J., George, C., 2006. Photosensitized reduction of nitrogen dioxide on humic acid as a source of nitrous acid. Nature 440, 195–198.
Stemmler, K., Ndour, M., Kleffmann, J., D'Anna, B., George, C., Bohn, B., et al., 2007. Light induced conversion of nitrogen dioxide into nitrous acid on submicron humic acid aerosol. Atmos. Chem. Phys. 7, 4237–4248.
Stutz, J., Alicke, B., Ackermann, R., Geyer, A., Wang, S.H., White, A.B., et al., 2004. Relative humidity dependence of HONO chemistry in urban areas. J. Geophys. Res.-Atmos. 109, D03307.
Su, H., Cheng, Y., Oswald, R., Behrendt, T., Trebs, I., Meixner, F., et al., 2011. Soil nitrite as a source of atmospheric HONO and OH radicals. Science 333, 1616–1618.
Stutz, J., Alicke, B., Neftel, A., 2002. Nitrous acid formation in the urban atmosphere: gradient measurement of NO_2 and HONO over grass in Milan, Italy. J. Geophys. Res. 107, LOP 5–1-5-10.
Su, H., Cheng, Y., Cheng, P., Zhang, Y., Dong, S., Zeng, L., et al., 2008. Observation of nighttime nitrous acid (HONO) formation at a non-urban site during PRIDE-PRD2004 in China. Atmos. Environ. 42, 6219–6232.
Tan, Z., Fuchs, H., Lu, K., Hofzumahaus, A., Bohn, B., Broch, S., et al., 2017. Radical chemistry at a rural site (Wangdu) in the North China Plain: observation and model calculations of OH, HO_2 and RO_2 radicals. Atmos. Chem. Phys. 17, 663–690.
Tan, Z., Rohrer, F., Lu, K., Ma, X., Bohn, B., Broch, S., et al., 2018. Wintertime photochemistry in Beijing: observations of ROx radical concentrations in the North China Plain during the BEST-ONE campaign. Atmos. Chem. Phys. 18, 12391–12411.
Tang, K., Qin, M., Duan, J., Fang, W., Meng, F., Liang, S., et al., 2019. A dual dynamic chamber system based on IBBCEAS for measuring fluxes of nitrous acid in agricultural fields in the North China Plain. Atmos. Environ. 196, 10–19.
Tang, K., Qin, M., Fang, W., Duan, J., Meng, F., Ye, K., et al., 2020. An automated dynamic chamber system for exchange flux measurement of reactive nitrogen oxides (HONO and NO_x) in farmland ecosystems of the Huaihe River Basin. China. Sci. Total Environ. 745, 140867.
Tang, Y., An, J., Wang, F., Li, Y., Qu, Y., Chen, Y., et al., 2015. Impacts of an unknown daytime HONO source on the mixing ratio and budget of HONO, and hydroxyl, hydroperoxyl, and organic peroxy radicals, in the coastal regions of China. Atmos. Chem. Phys. 15, 9381–9398.
Tsai, C., Spolaor, M., Colosimo, S.F., Pikelnaya, O., Cheung, R., Williams, E., et al., 2018. Nitrous acid formation in a snow-free wintertime polluted rural area. Atmos. Chem. Phys. 18, 1977–1996.
VandenBoer, T.C., Brown, S.S., Murphy, J.G., Keene, W.C., Young, C.J., Pszenny, A.A.P., et al., 2013. Understanding the role

of the ground surface in HONO vertical structure: high resolution vertical profiles during NACHTT-11. J. Geophys. Res.-Atmos. 118, 10155–10171.
VandenBoer, T.C., Markovic, M.Z., Sanders, J.E., Ren, X., Pusede, S.E., Browne, E.C., et al., 2014a. Evidence for a nitrous acid (HONO) reservoir at the ground surface in Bakersfield, CA, during CalNex 2010. J. Geophys. Res.-Atmos. 119, 9093–9106.
VandenBoer, T.C., Young, C.J., Talukdar, R.K., Markovic, M.Z., Brown, S.S., Roberts, J.M., et al., 2014b. Nocturnal loss and daytime source of nitrous acid through reactive uptake and displacement. Nat. Geosci. 8, 55–60.
Villena, G., Kleffmann, J., Kurtenbach, R., Wiesen, P., Lissi, E., Rubio, M.A., et al., 2011. Vertical gradients of HONO, NO_x and O_3 in Santiago de Chile. Atmos. Environ. 45, 3867–3873.
Wang, J., Zhang, X., Guo, J., Wang, Z., Zhang, M., 2017. Observation of nitrous acid (HONO) in Beijing, China: seasonal variation, nocturnal formation and daytime budget. Sci. Total Environ. 587-588, 350–359.
Wang, S.S., Zhou, R., Zhao, H., Wang, Z.R., Chen, L.M., Zhou, B., 2013. Long-term observation of atmospheric nitrous acid (HONO) and its implication to local NO_2 levels in Shanghai, China. Atmos. Environ. 77, 718–724.
Weber, B., Wu, D., Tamm, A., Ruckteschler, N., Rodríguez-Caballero, E., Steinkamp, J., et al., 2015. Biological soil crusts accelerate the nitrogen cycle through large NO and HONO emissions in drylands. Proc. Natl. Acad. Sci. USA 112, 15384–15389.
Western Plant Health Association, 2002. Western Fertilizer Handbool, 9th Edn. Waveland Press, Inc., Long Grove, Illinois, U.S.
Wong, K.W., Tsai, C., Lefer, B., Grossberg, N., Stutz, J., 2013. Modeling of daytime HONO vertical gradients during SHARP 2009. Atmos. Chem. Phys. 13, 3587–3601.
Wu, D., Horn, M.A., Behrendt, T., Muller, S., Li, J., Cole, J.A., et al., 2019. Soil HONO emissions at high moisture content are driven by microbial nitrate reduction to nitrite: tackling the HONO puzzle. ISME J. 13, 1688–1699.
Xue, C., Ye, C., Zhang, Y., Ma, Z., Liu, P., Zhang, C., et al., 2019. Development and application of a twin open-top chambers method to measure soil HONO emission in the North China Plain. Sci. Total Environ. 659, 621–631.
Xue, C., Ye, C., Zhang, C., Catoire, V., Liu, P., Gu, R., et al., 2021. Evidence for strong HONO emission from fertilized agricultural fields and its remarkable impact on regional O_3 pollution in the Summer North China Plain. ACS Earth Space Chem. 5, 340–347.
Xue, C., Zhang, C., Ye, C., Liu, P., Catoire, V., Krysztofiak, G., et al., 2020. HONO budget and its role in nitrate formation in the rural North China Plain. Environ. Sci. Thchnol. 54, 11048–11057.
Yang, Q., Su, H., Li, X., Cheng, Y., Lu, K., Cheng, P., et al., 2014. Daytime HONO formation in the suburban area of the megacity Beijing, China. Science China Chem. 57, 1032–1042.
Ye, C., Zhang, N., Gao, H., Zhou, X., 2017. Photolysis of particulate nitrate as a source of HONO and NO_x. Environ. Sci. Technol. 51, 6849–6856.
Ye, C., Zhou, X., Pu, D., Stutz, J., Festa, J., Spolaor, M., et al., 2018. Tropospheric HONO distribution and chemistry in the southeastern US. Atmos. Chem. Phys. 18, 9107–9120.
Ye, C., Zhou, X., Pu, D., Stutz, J., Festa, J., Spolaor, M., et al., 2016. Rapid cycling of reactive nitrogen in the marine boundary layer. Nature 532, 489–491.
Yu, Y., Galle, B., Panday, A., Hodson, E., Prinn, R., Wang, S., 2009. Observations of high rates of NO_2-HONO conversion in the nocturnal atmospheric boundary layer in Kathmandu, Nepal. Atmos. Chem. Phys. 9, 6401–6415.
Zhang, N., Zhou, X., Bertman, S., Tang, D., Alaghmand, M., Shepson, P.B., et al., 2012. Measurements of ambient HONO concentrations and vertical HONO flux above a northern Michigan forest canopy. Atmos. Chem. Phys. 12, 8285–8296.
Zhang, W., Tong, S., Jia, C., Wang, L., Liu, B., Tang, G., et al., 2020. Different HONO sources for three layers at the urban area of Beijing. Environ. Sci. Technol. 54, 12870–12880.
Zhang, W., Tong, S., Ge, M., An, J., Shi, Z., Hou, S., et al., 2019. Variations and sources of nitrous acid (HONO) during a severe pollution episode in Beijing in winter 2016. Sci. Total Environ. 648, 253–262.
Zhou, X., Civerolo, K., Dai, H., Huang, G., Schwab, J., Demerjian, K., 2002. Summertime nitrous acid chemistry in the atmospheric boundary layer at a rural site in New York State. J. Geophys. Res. - Atmos. 107, 4590.
Zhou, X., Gao, H., He, Y., Huang, G., Bertman, S.B., Civerolo, K., et al., 2003. Nitric acid photolysis on surfaces in low-NO_x environments: significant atmospheric implications. Geophys. Res. Lett. 30, 2217.
Zhou, X., Zhang, N., TerAvest, M., Tang, D., Hou, J., Bertman, S., et al., 2011. Nitric acid photolysis on forest canopy surface as a source for tropospheric nitrous acid. Nat. Geosci. 4, 440–443.